# Characterization of Porous Cellulose Triacetate Derived from Kapok Fibres (Ceiba pentandra) as a Tool to Enhance Crude Oil Absorption

**Larsen Alessandro**
UCSI University, Federal Territory of Kuala Lumpur
**Eric Wei Chiang Chan**
UCSI University, Federal Territory of Kuala Lumpur
**Juhana Jaafar**
Universiti Teknologi Malaysia
**John Beardall**
Monash University
**Michelle Oi Yoon Soo** ( michellesoo@ucsiuniversity.edu.my )
UCSI University, Federal Territory of Kuala Lumpur

**Research Article**

**Keywords:** Cellulose triacetate, porous CTA, kapok fibres, acetylation, membrane additive, PVDF/CTA membrane

**Posted Date:** October 12th, 2023

**DOI:** https://doi.org/10.21203/rs.3.rs-3415579/v1



**Additional Declarations:** No competing interests reported.

# Abstract

Kapok fibre is a natural fibre obtained from the seed pods of the kapok tree (*Ceiba pentandra*). Cellulose triacetate (CTA) is a cellulose derivative in which hydroxyl groups of cellulose were converted into acetyl groups. In this study, high purity cellulose was extracted from kapok fibres and was converted to CTA. The produced CTA showed a high degree of substitution (DS) (2.9) by titration, which was confirmed by $^{1}$H- and $^{13}$C-NMR. CTA was soluble in non-polar chloroform and the conversion of hydroxyl groups into acetyl groups was confirmed by Fourier Transform Infrared Spectroscoy (FTIR). From Thermogravimetric Analysis-Differential Scanning Calorimetry (TGA-DSC) results, CTA is thermally more stable than delignified kapok fibre where at the same time, CTA needed more energy to crystallize. X-Ray Diffraction (XRD) showed the decrease in crystallinity of CTA compared to delignified kapok fibre due to the presence of acetyl groups. Visually, CTA produced is irregular in shape and porous. $^{1}$H-NMR and $^{13}$C-NMR were used to confirm the CTA produced by looking at the molecular conformation. CTA from kapok exhibited stability in higher temperature, is porous and less crystalline than unmodified cellulose. CTA significantly increased the porosity of PVDF membranes, thereby enhancing its oil absorption capacities and suggesting that CTA is suitable as an additive to improve the properties of a membrane that is specifically designed for oil spill remediation.


# Introduction

Cellulose is one of the most abundant polymers found in nature with admirable properties such as being biodegradable and non-toxic and it can be considered a renewable resource (de Freitas et al. 2017). Much research has investigated the properties of cellulose derivatives such as cellulose acetate, cellulose nitrate, methyl cellulose, hydroxy ethyl cellulose and many more. Prior to further modification, cellulose is usually isolated from lignocellulose, comprising lignin and hemicellulose (R. Kumar et al. 2017).

Cellulose acetate (CA) is one of the most explored cellulose derivatives as it can be used to produce membranes, cigarette filters, films, and is even incorporated in pharmaceutical products (H. Zhou et al. 2021). CA is produced by replacing one to three hydroxyl groups in the anhydroglucose unit of CA with acetyl group(s). One replacement of hydroxyl group would produce cellulose monoacetate (commonly also referred to as CA), while two and three replacements would produce cellulose diacetate (CDA) and cellulose triacetate (CTA) respectively (S. Zhang et al. 2022). By converting cellulose to CA, the chemical, physical, mechanical, and morphological characteristics are affected. The replacement is usually done by reacting cellulose with glacial acetic acid as a solvent, acetic anhydride as the acetylating agent and sulphuric acid as a catalyst (Battisti et al. 2018). Some improvements and innovations have been made such as replacing acetic acid with ionic liquids (ILs) as green solvent (Battisti et al. 2018) and using iodine as a catalyst (Nemr et al. 2017).

Substitution of hydroxyl to acetyl groups alters the solubility of CA in different solvents. Cellulose is insoluble in common organic and aqueous solvents due to strong hydrogen bonding within its structure

(Suzuki et al. 2018). On the other hand, CDA is soluble in acetone or tetrahydrofuran (THF) and CTA is soluble in chloroform, dichloromethane and other chlorinated solvents (de Freitas et al. 2017).

CTA is often used as a material in reverse-osmosis membranes and textile fibres due to properties such as having good thermoplasticity, being non-toxic, low flammability and its strong mechanical properties (El Nemr et al. 2015; Jia et al. 2022). CTA has a degree of substitution (DS) of above 2.8 which indicates that at least 2.8 hydroxyl groups per anhydroglucose unit in the cellulose are converted into acetyl groups (Wolfs & Meier 2021). By converting hydroxyl groups into acetyl groups, the hydrophobicity-oleophilicity of CTA will be higher compared to cellulose or cellulose monoacetate. Thus, incorporating CTA with another hydrophobic polymer in making blended polymer membranes could prove to be useful to remediate hydrophobic pollutants such as those that occur in crude oil spills.

As cellulose is traditionally extracted from wood, finding alternatives that are cheaper and have less environmental impacts are crucial. One of the native plants in Malaysia which has a high percentage (around 69%) of cellulose is kapok. Kapok (*Ceiba pentandra*) or *kekabu* as it is commonly known in Malaysia is the tallest tree among the *Ceiba* species (Chan et al. 2022). It was first planted in Africa and was introduced to tropical Asia where presently it is highly abundant in Indonesia, Malaysia, and Thailand. It is also found in South America (Kang et al. 2022). Matured kapok trees can bear hundreds of pods filled with fibrous seeds. Traditionally, the fibre is used to stuff pillows and as the internal material for cloth-based dolls. These fibres are also moisture-resistant, quick-drying, resilient and buoyant (Rahmah & Abdullah 2011). Nevertheless, the hydrophobicity-oleophilicity property of kapok fibres has made it a good oil absorbent (Zheng et al. 2015). This property comes from the natural acetyl group substituents (2–4%, higher than other natural fibres) and from the waxy layer of the fibre (Rahmah & Abdullah 2011).

As compared with flax (*Linum usitatissimum*), ramie (*Boehmeria nivea*), and jute (*Corchorus capsularis*) where porosity is 77%, 70.4%, and 70%, respectively, kapok fibres distinct itself with its large lumen and thin cell walls that give porosity of more than 80% (Xiang et al. 2013; W. D. Yang & Li 2012). It has been shown that kapok fibres have obvious porous structures that are distributed widely across the fibres with most of them having a diameter less than 0.3 μm (Z. Yang et al. 2018). Other than being fast-growing, a high porosity would be one of the advantages to produce porous cellulose triacetate from kapok fibres (Mohamed et al. 2017; Nordahlia et al. 2016).

In this study, porous-hydrophobic CTA was produced with the intention of incorporating it into a PVDF membrane to act as an absorbent of crude oil and, in the future, to act as a carrier of oil-degrading bacteria for the simultaneous biological degradation of oil. Hence, the present research undertakes a thorough and comprehensive characterization of cellulose triacetate (CTA) derived from kapok fibres. The primary objective of this study was to gain an in-depth and nuanced understanding of the potential utility of porous CTA as a reinforcement component within polymer composites. The characterization methods include FTIR that was used to observe the replacement of hydroxyl into acetyl groups, titration and H-NMR to observe the degree of substitution, thermogravimetric analysis (TGA) and differential scanning

calorimetry (DSC) to measure the changes in properties as the CTA product was heated, a solubility test to confirm the nature of the produced CTA, XRD to determine the crystallinity of the CTA, FeSEM to capture the structure of CTA and H- and C-NMR to determine its molecular structure. Lastly, the porosity of PVDF membranes, blended with different CTA concentrations, was also determined, followed by preliminary tests on its crude oil absorption capacity.

## Materials and method

# Chemicals and materials

Kapok fibres were obtained from a textile shop in Teluk Intan, Perak, Malaysia. Sodium hydroxide (NaOH) pellet, dimethyl sulfoxide (DMSO), dichloromethane, acetic acid (glacial) 100%, sulfuric acid, acetic anhydride “for synthesis” grade, chloroform, hydrochloric acid fuming 37% and acetone were purchased from Merck (USA). Hydrogen peroxide was purchased from Inscent (Malaysia). Ethyl alcohol 95% (v/v)-denatured was purchased from Systerm (Malaysia). Minitab (USA) was used for statistical analyses.

# Cellulose extraction

Cellulose was extracted from kapok fibres in two steps, namely delignification and bleaching (Tristantini & Sandra 2018). Delignification was done by adding 120 mL of 17.5% NaOH into an Erlenmeyer flask containing 3 g of cleaned kapok fibre. The flask was then covered with aluminium foil and incubated in a water bath (90 $^{o}$C) for 3 hours. For the first 30 minutes, the kapok fibre was pressed frequently to allow it to become fully immersed in the hot NaOH solution. Once the kapok fibre was fully immersed, it was pressed and stirred occasionally for the remaining time. After 3 hours, the delignified kapok fibre was then removed from the flask and was washed twice with distilled water until a neutral pH was achieved. The delignified kapok fibre was then hand-squeezed and dried in a 60 $^{o}$C oven overnight. 1.5 g of dried delignified kapok fibre was then bleached using 60 mL of 10% hydrogen peroxide ($H_2O_2$). It was covered by aluminium foil and heated in a water bath at 90 $^{o}$C for 15 minutes. The material was then removed and washed twice with distilled water until a neutral pH was achieved. The bleached kapok fibre was then dried in a 60 $^{o}$C oven overnight.

# Acetylation of cellulose

Acetylation was adapted from Yunita et al. (2018). 2 grams of bleached kapok fibre were activated in a flask containing 50 mL of acetic acid, covered by aluminium foil and heated in a 50 $^{o}$C water bath for 30 minutes. A mixture of 0.32 mL of sulphuric acid and 18 mL of acetic acid was then added into the flask and heated continuously for 30 minutes. Acetylation was initiated by adding 48 mL of acetic anhydride. It was then heated for 45 minutes under continual stirring. The solution was then allowed to cool down for 10 minutes before adding it dropwise into 850 mL of distilled water with continual stirring. The precipitated cellulose triacetate (CTA) was then filtered using Whatman® filter paper no 1 and washed with water until a neutral pH was achieved. It was then dried in a 60 $^{o}$C oven overnight. The dried CTA was ground by pushing it through a metal sieve.

# Degree of substitution (DS) determination

Determination of the degree of substitution was done using a titration method adapted from de Freitas et al. (2017). CTA was dried in an oven (60 $^{o}$C) overnight. 20 mL of 75% ethanol was added into a flask containing 0.1 g of CTA. This was covered by aluminum foil and heated for 30 minutes in a 60 $^{o}$C water bath. 25 mL of 0.1 M NaOH was then added into the mixture and heated at the same temperature for 15 minutes. It was then allowed to cool down and stand for 48 hours. The excess NaOH was then titrated using a standardized 0.1 M hydrochloric acid (HCl) solution. The DS was calculated as below (Eqs. 1 and 2) (Rahim et al. 2017):

$$\%\text{Acetyl} = \frac{[(Blank - Sample) * HClMolarity * 0.043 * 100]}{Sampleweight} \quad (1)$$

$$\mathbf{DS} = \frac{(162 * \%Acetyl)}{[4300 - (42 * \%Acetyl)]} \quad \mathbf{(2)}$$

# Characterization of CTA

Characterizations in terms of physicochemical and thermal properties were done using the following tests: solubility test, FTIR, TGA, DSC, XRD, FeSEM, C-NMR and H-NMR. CTA was ground, and all samples were dried overnight in 60°C oven prior to analysis.

# Solubility test

Solubility tests were done by adding 0.1 g of CTA into 20 mL of different solvents and stirring for 10 minutes. The solvents were chloroform, dichloromethane, acetone, distilled water, acetic acid and DMSO. The solubility of CTA in the solvents was observed by eye.

# Fourier transform infrared spectroscopy (FTIR)

Molecular compounds of raw kapok fibres, delignified kapok fibres and CTA were observed using Shimadzu (Japan) IR Tracer 100. FTIR was let to blank the background noise that might contaminate the peaks produced prior to analysis. The spectra were recorded in the wavenumber range of 4000 – 500 $cm^{-1}$ with resolution of 4 $cm^{-1}$.

# Thermal analysis

Thermal analyses of the raw kapok fibres, delignified kapok fibres and CTA were done using a Mettler Toledo TGA-DSC HT 3, while delignified kapok and CTA were subjected to Q50 thermogravimetric analysis (TGA) using Shimadzu (Japan) DSC-60 and TA instruments (USA). 5–10 mg of samples were taken for TGA analysis, whereby 6–12 mg of samples were used for the DSC.

# X-Ray diffractometer (XRD)

Crystallographic structures, chemical composition, and physical properties of the raw kapok fibers, delignified kapok and CTA were analysed by Malvern Panalytical (UK) Empyrean X-Ray diffractometer (XRD). Samples were flattened on the sample holder to get the best results.

# Field emission scanning electron microscopy (FeSEM)

A Hitachi (Japan) SU8010 was used to observe the microstructure of raw kapok, delignified kapok and CTA. All samples were sputter-coated with a thin film of gold (6 nm) using a Quorum Q150R S.

### *$^{13}$C-NMR and $^{1}$H-NMR*

Compound analysis of CTA was done using a Bruker (USA) AVANCE NEO 300 MHz NMR Spectrometer. 20 mg of CTA was dissolved with 600 µL deuterated chloroform ($CDCl_3$). It was then transferred into an NMR tube for analysis. Degree of substitution was determined using the following equation in $^{1}$H-NMR (Eq. 3):

$$DS = \frac{7 \times I\,(acetyl)}{3 \times I\,(AGU)}$$

3

I(acetyl) is the integral of methyl protons of acetyl groups; I(AGU) is the integral of all protons of an anhydroglucose unit.

# Production of PVDF/CTA membrane

The dope solution of poly(vinylidene fluoride)/cellulose triacetate (PVDF/CTA) in N, N-dimethylacetamide (DMAc) with a total of 50 g was made following the details in Table 1. It was then casted on a glass plate with tapes as the frame, with a thickness of 176 micrometers. The membrane was formed using a technique called non-solvent induced phase separation (NIPS) with water as the non-solvent. It was immersed in water overnight before use to ensure complete solvent exchange. It was kept in boiled water to minimize the biofilm formation and the water was changed weekly.

Table 1
Composition of dope solution of PVDF/CTA membrane. Membranes with asterisk (*) were chosen for further crude oil absorption test.

| Name | Concentration of CTA | PVDF (g) | DMAc (g) | CTA (g) |
|---|---|---|---|---|
| PC0* | 0% | 9 | 41 | 0 |
| PC0.01* | 0.01% | 9 | 40.995 | 0.005 |
| PC0.05 | 0.05% | 9 | 40.975 | 0.025 |
| PC0.1 | 0.1% | 9 | 40.95 | 0.05 |
| PC0.5* | 0.5% | 9 | 40.75 | 0.25 |
| PC1 | 1% | 9 | 40.5 | 0.5 |
| PC2 | 2% | 9 | 40 | 1 |
| PC3* | 3% | 9 | 39.5 | 1.5 |
| PC4 | 4% | 9 | 39 | 2 |
| PC5 | 5% | 9 | 38.5 | 2.5 |

# Porosity test of PVDF/CTA membrane

3 cm x 3 cm of PVDF/CTA membrane was dried in a 40°C oven until a constant weight was achieved. Weights of wet and dry membranes were recorded and incorporated into the formula of Velu et al. (2015) to determine the porosity (Eq. 4) as follows:

$$Porosity\,(\%) = \frac{(W_{wet} - W_{dry})}{\rho_{water} \times V_T} \times 100$$

4

$W_{wet}$ is weight of wet membrane (g); $W_{dry}$ is weight of dry membrane; $\rho_{water}$ is density of water (0.997 g/cm3); $V_T$ is membrane volume in wet state ($cm^3$)

# Crude oil absorption test

The membrane was cut into a circle with a diameter of 5.5 cm. It was then taken from the water and held with forceps vertically for 3 minutes before weighing it and immersing it into a container containing 10 mL of crude oil. It was then shaken in a shaking incubator at 200 rpm at 30°C for 24 hours. Prior to extracting the crude oil from the membrane, it was taken out and held with forceps vertically for 3 minutes to ensure that the unabsorbed crude oil wouldn't influence the results. The membrane containing crude oil was then extracted with hexane. After the extraction, the membrane was then dried in 60°C oven overnight. The absorption capacity (Eq. 5) of each membrane was measured using the formula:

$$\%Absorption = \frac{W_{crudeoil}}{W_o} \times 100$$

5

$W_{crudeoil}$ is weight of the crude oil extracted from the membrane; $W_o$is weight of the dry membrane.

## Results and Discussion

# Production of cellulose triacetate (CTA)

Alkali treatment was used to delignify the raw kapok fibres (Fig. 1a). Delignification is meant to remove lignin from the lignocellulosic material of kapok fibres. Lignin is a complex polymer found in plant cell walls which provides rigidity and strength to the fibres. However, lignin is generally removed since it can interfere with the acetylation process. Lignin may hinder the acetylating agents to reach the cellulose surface and react with the hydroxyl groups due its bulky and three-dimensional structure (A. Kumar et al. 2021). It can also compete with cellulose for acetylation thus making CTA formation less efficient. Furthermore, the presence of hydrogen bonding and other interactions leads to strong bonding between lignin and cellulose, resulting in the formation of lignin-cellulose complexes (Y. Yuan et al. 2021) thereby limiting the extent of acetylation.

Strong alkaline is usually employed to break down the lignin structure and dissolve it by hydrolysis and solubilization processes. Hemicellulose was removed as well during delignification as it is soluble in strong alkaline solution. 17.5% of NaOH was used as this is the maximum concentration that can be used without degrading α-cellulose (Susi et al. 2023; Tristantini and Sandra 2018). Hydroxide ions react with ester and ether bonds of lignin causing it to depolymerize and become soluble (Joshi et al. 2022). After lignin, which gives a brownish colour to the fibres, is removed, the kapok fibres became a lighter brown in colour (Fig. 1b). The changes in colour of the fibres in this study agree with the observations of Susi *et al*. (2023), which indicates that the colour is heavily dependent on the treatments such as duration and intensity of the solution used (Susi et al. 2023).

Delignification was followed by bleaching that further removed more impurities and improved the appearance from lighter brownish to yellowish-white (Fig. 1c). Hydrogen peroxide ($H_2O_2$) was used as it is generally considered safe and environmentally friendly. This treatment broke down chromophores, which are responsible for the coloration of kapok fibres, through oxidative reactions (Estefania & Loor 2022). The yellowish coloration in the delignified kapok fibres was due to the presence of remaining impurities, residual lignin and other components that could not be removed completely. Overbleaching may affect the structural integrity and weaken the fibres.

The delignified kapok fibres were then acetylated to produce cellulose triacetate (CTA) (Fig. 1d). Acetylation is a chemical modification process whereby hydroxyl groups (-OH) are converted into acetyl groups (-$COCH_3$) making the resulting cellulose triacetate more hydrophobic with enhanced thermal stability and increased chemical resistance (Dong et al. 2017). Delignified kapok fibres were activated

using acetic acid to increase the reactivity of the hydroxyl groups, thus enabling better acetyl group attachment. Acetic anhydride, as an acetylating agent, reacted with the activated hydroxyl groups resulting in the substitution of hydroxyl groups into acetyl groups via esterification reactions. The produced CTA was then precipitated in water since it is insoluble in water due the presence of non-polar groups. Three grams of CTA were produced from two grams of delignified kapok fibres due to the incorporation of acetyl groups which have higher molecular weight than hydroxyl groups. CTA was then further validated by titration, FTIR and solubility test.

# Degree of substitution (DS) by titration

Degree of substitution (DS) is a variable to measure the number of acetyl groups that replace hydroxyl groups in one anhydroglucose unit (AGU) in cellulose. Cellulose triacetate has a DS of 2.8–3 indicating that by average, 2.8 to 3 acetyl groups are present in one AGU (Fei et al. 2017). The produced CTA had a DS of 2.89 indicating that it is cellulose triacetate compared to raw kapok fibres which has a DS of 0.07 (Table 2). A few previous studies have also obtained similar DS values for cellulose triacetate (Hindi & Abohassan 2015; Jia et al. 2022; Nemr et al. 2017; X. Zhang et al. 2023). DS greatly influenced the properties of cellulose triacetate such as solubility, thermal stability, and mechanical properties (X. Zhou et al. 2016). As the DS increases, the solubility of CTA in nonpolar solvents increases, becoming more resistant to thermal degradation, increasing the stiffness, and reducing the flexibility of the material.

Table 2
Degree of substitution (DS) of raw kapok and CTA.

| Sample | Degree of Substitution |
|---|---|
| Raw kapok | 0.07 |
| CTA | 2.89 |

# Confirmation of delignification and acetylation

FTIR spectra of raw kapok fibres, delignified kapok fibres and CTA are shown in Fig. 2. A broad peak in the range of 3300–3600 $cm^{-1}$ shows stretching vibrations of hydroxyl groups where it appeared in raw kapok fibres and delignified kapok fibres but was absent in CTA. This shows that acetylation was successfully done to convert hydroxyl groups to become acetyl groups. The sharp rise in peaks at 1732 $cm^{-1}$ is present in the CTA as compared with raw and delignified kapok fibres since acetyl groups are composed of carbonyl groups. The decrease of carbonyl groups peaked at 1732 $cm^{-1}$ in delignified kapok fibres, as compared with raw kapok fibres, indicating that the removal of hemicellulose may contain acetyl groups or other carbonyl functionalities. Peaks at 1032 $cm^{-1}$ indicate stretching vibrations of C-O bond in hemicellulose which are reduced in delignified kapok fibres but increased sharply in CTA due to the introduced acetyl groups. Lignin-specific peaks were observed around 1200–1600 $cm^{-1}$ and were reduced in delignified kapok fibres as they represent aromatic skeletal vibrations and C-H

deformations in aromatic rings found in lignin. Lastly, a C-H peak at 1368 $cm^{-1}$ was observed in CTA as this is also found in the acetyl groups. Similar observations were also reported previously (de Melo Brites et al. 2020; Nabili et al. 2017; Shaikh et al. 2022).

# Solubility of CTA in solvents

The degree of substitution of CTA could further be clarified by immersing CTA into different solvents to test its solubility. Solubility is determined by factors like polarity, hydrogen bonding, and intermolecular forces. The solubility of CTA is shown in Table 3. Common solvents to differentiate CTA from cellulose diacetate (DS 2.2–2.6) or monoacetate (DS ± 1) are chloroform, acetone, and water. CTA dissolved in chloroform but not in acetone and water (Hindi & Abohassan 2015). CTA also dissolved in dichloromethane and dimethylsulfoxide (DMSO) (Jogunola et al. 2016). Chloroform and dichloromethane are non-polar, chlorinated solvents whereby they have good solvating power for the hydrophobic acetyl groups in CTA. DMSO is a polar aprotic solvent known for its strong ability to form hydrogen bonds that interacts with acetyl groups of CTA thus facilitating dissolution. CTA is partially soluble in glacial acetic acid, a polar solvent, due to the ability of the glacial acetic acid to form hydrogen bonds with acetyl groups due to the presence of carboxyl (COOH) groups and also disrupt the intermolecular hydrogen bonding between CTA chains, allowing a certain extent of dissolution (Tristantini & Sandra 2018). On the other hand, acetone and water as polar solvents could not dissolve CTA due to their polarity (Wsoo et al. 2020). The lack of hydroxyl groups and the presence of acetyl groups, which are non-polar, in CTA render it insoluble in water due to the inability to form strong hydrogen bonds with water. This is because water also has a high degree of hydrogen bonding making CTA form aggregates or become precipitated instead. Hydrophobic acetyl groups do not readily interact with polar solvents through hydrogen bonding or favourable polar interactions; instead, they dominate the intermolecular interactions and prevent efficient dissolution in both water and acetone.

# Thermal properties

# Thermal decomposition study of CTA

Figure 3a shows the thermal stability and decomposition behaviour of raw kapok fibres. 4.2% of the weight of raw kapok fibres was lost between 24°C to 109°C due to loss in moisture whereby the major decomposition happened between 225°C and 384°C. The major decomposition caused a significant reduction in weight (57.6%) which peaked at 354°C. There was another decomposition (loss of 15.9% of weight) that peaked at 426°C. By looking at the weight loss as compared with the previous decomposition, this 426°C decomposition suggests the presence of lignin which is a complex and highly cross-linked polymer. Kapok comprises of 35–50% of cellulose, 15–22% of lignin, and 22–45% of hemicellulose (Purnawati et al. 2018).

Generally, thermal degradation of lignocellulosic materials starts with loss of water content followed by depolymerization of hemicellulose, lignin, and cellulose (Sartika et al. 2020). If the heating continues up to 600°C, oxidation, and production of low molecular weight gases due to the breakdown of carbon

residues may happen. If the lignin content is still high, the degradation of lignin may also happen at a very high temperature (400–600°C) (Jun Poon et al. 2020). The degradation in the second stage started with the degradation of hemicellulose which has lower thermal stability, followed by cellulose. Degradation of cellulose produces anhydrocellulose, levoglucosan and some other volatile compounds. Anhydrocellulose is a dehydrated form of cellulose whereby levoglucosan is a cyclic anhydrosugar. However, these 2 compounds cannot be detected using TGA, instead pyrolysis-GC-MS is required to detect them. Above 370°C, the curve is generally flattened due to the formation of char. This carbon-rich material remained after the thermal decomposition of cellulose.

Thermogravimetric curves of delignified kapok fibres are shown in Fig. 3b. A slight loss in weight (3.96%) was observed in between 50 and 240°C due to the loss in water whereby the very noticeable decomposition of delignified kapok fibres occurs at around 240°C to 370°C. In the latter, the delignified kapok fibres lost around 74% of its weight with the maximum weight loss rate occurring at 350°C ($T_{max}$). Onset of the cellulose degradation started at 240°C. Small peaks were observed between 400–600°C due to the presence of small amounts of lignin. A previous study has also shown two stages of thermal degradation i.e. 50–358°C (loss of 39.79%) and 358–600°C (loss of 36.96%) with $T_{max}$ of 331.3°C (Sartika et al. 2020). As compared to previous studies, a higher $T_{max}$ showed that the produced delignified kapok fibre was more stable against thermal degradation. Similarly, a study showed that delignified kapok fibres with $T_{max}$ of 350°C indicated a much higher purity of cellulose than raw kapok fibres (Jun Poon et al. 2020). In another study, the alkali-treated kapok fibres had similar thermal stability where decomposition started at 352°C (Danial Jamat & Asik 2019). The difference in the thermal degradation may be due to the delignification methods and chemicals used which resulted in different purity of cellulose produced.

In Fig. 3c, shows TGA-DTG curves of cellulose triacetate extracted from kapok fibres. There was a slight loss curve between 50–290°C due to the removal of moisture in the CTA. Generally, CTA had a higher thermal stability as compared with delignified kapok fibres. For instance, the decomposition of CTA started at 289°C instead of 240°C in delignified kapok fibres and even though the maximum weight loss occurred at a slightly lower temperature (345°C), CTA lost most of its weight (74%) in higher temperature within the range of 300–400°C. This showed that by converting kapok fibre into CTA, the thermal stability improved. $T_{max}$ of CTA in this research was lower than that of commercial CTA (378°C) and the CTA (382°C) synthesized in another study where the cellulose was extracted from date palm trunk mesh fibres (Shaikh et al. 2022). This was due to different sources of cellulose where different biomass will have different degree of crystallinity and molecular weight, thus reflecting different thermal stability (Mittal et al. 2011). For instance, CTA made from corn-stover cellulose had a maximum decomposition temperature of 366°C (Jia et al. 2022). Another example is CTA from microfibrillated date seeds cellulose that had an almost similar $T_{max}$ (372°C) to the previous study.

# Thermal stability study of CTA

Differential scanning calorimetry (DSC) curves of raw kapok fibres, delignified kapok fibres and CTA were shown in Fig. 4a, 4b, and 4c, respectively. In Fig. 4a, one exothermic peak at 326°C was likely associated with a major decomposition of the major components of raw kapok fibres which is cellulose. Exothermic peaks of decomposition of lignin were expected to appear at 205°C and 278°C but they were absent (Guo et al. 2016). This might happen due to the insignificant decomposition process that resulted in it not being detected by the DSC. It is also possible that waxes or any impurities contained in the raw kapok fibres may not significantly affect the thermal properties and were thus also not detected by the DSC.

As shown in Fig. 4b, DSC detected one sharp crystallization peak in delignified kapok fibres at 165°C with an enthalpy of crystallization (ΔHcrys) of 129.95 J/g. A sharp and tall peak represents a high degree of crystallinity. Another study showed exothermic peaks of treated kapok fibres appearing at much higher temperatures where they are divided into 2 steps, degradation of cellulose (300–350°C) and oxidation of char (400–450°C) (Fauziah Syed Draman et al. 2014). In the same study, the first exothermic peak appeared at 330°C which was much higher than this study could be due to different pre-treatment methods resulting in different crystallinity and trace elements remaining.

In addition, CTA (Fig. 4c) presented a few distinctive peaks, two exothermic and one endothermic. One exothermic peak at 151°C represented the crystallization of CTA with a ΔHcrys of 171.91 J/g. The crystallization happened at lower temperature than the delignified kapok fibres, however, the ΔHcrys indicated that it requires more energy for the acetyl groups and the cellulose chain to form an ordered lattice. The acetyl groups promote stronger intermolecular bonds thus increasing the organization of the polymer chains in the crystalline regions. In addition, there was a small endothermic peak at 182°C which relates to structural rearrangements of CTA after crystallization where it required 6.06 J/g of energy. The last exothermic peak was at 293°C, depicting thermal degradation where CTA released 28.08 J/g of energy during the breaking of acetyl groups from the cellulose backbone. For CTA synthesized from microfibrillated date seeds cellulose, there were 2 endothermic peaks, instead of exothermic peaks. The 2 peaks showed outflow of water at 72°C and melting of crystalline regions of CTA at 245°C. This shows that CTA made from kapok fibres had lower crystallinity as compared to CTA from microfibrillated date seeds cellulose (Nabili et al. 2017).

# Crystallinity properties

The X-ray diffraction (XRD) results indicating the crystallinity of raw kapok fibres, delignified kapok fibres and cellulose triacetate are shown in Fig. 5. In Fig. 5a, peaks indicating crystalline diffraction appear at 14.7°, 23.1° and 34.5° which are associated with (110), (200) and (004) crystallographic planes that are the typical characteristics of a type I cellulose crystal structure (Nindiyasari et al. 2016; Sartika et al. 2020). A diffraction peak at 14.7° indicated the scattering of X-rays by the regularly arranged cellulose chains along this plane. The peak at 23.1° indicated the amorphous part of cellulose with the presence of an organized stacking of cellulose chains in the lattice along the plane (Boukir et al. 2019). The 34.5° peak showed the arrangement of cellulose chains in the lattice along this specific plane (X. Yuan & Cheng 2015). Lignin in the raw kapok fibres had corresponding peaks at 16.8° and 22.8°. These were similar to

study done by Gomide et al. (2020). However, peaks at 43.5° and 63.9° have not been clearly defined by other studies. They might correspond to the aluminium sample holder (Gomide et al. 2020) or to residual fractions (Bouramdane et al. 2022).

Similarly raw kapok fibres, as with delignified kapok fibres (Fig. 5b), contain a high purity of cellulose, and show similar peaks at 15.1°, 23.2° and 34.9° which are typical peaks indicating native/crystalline cellulose. The presence of acetyl groups in CTA produced broader and less defined diffraction peaks (Fig. 5c) as compared to cellulose due to the scattering from the disordered or amorphous regions of CTA. Acetyl groups disrupt the regular arrangement of cellulose chains thus reducing the degree of crystallinity. Disappearance of peaks in CTA would mean loss of crystallinity as compared with delignified kapok fibres that had sharper peaks. The change was due to the substitution of hydroxyl groups by acetyl groups which have a larger volume along the axes. Diffraction peaks of CTA were located at 8.3° which is known to derive from semi-crystalline acetylated derivatives cellulose due to an increase in the interfibrillar distance caused by the presence of the acetyl groups along cellulose chains (Cobo et al. 2017). The peak at 10.8° corresponded to the (110) crystallographic plane indicating the presence of ordered stacking of cellulose chains along this specific plane in the CTA lattice, whilst the 17.4° peak represented the amorphous region of CTA. 17°, 22° and 35° peaks are commonly associated with cellulose triacetate (Cobo et al. 2017; Nu et al. 2019).

# Confirmation of acetyl groups presence in CTA

$^{1}$H-NMR spectra of cellulose triacetate are shown in Fig. 6a. $^{1}$H-NMR analysis was done to confirm the presence of acetyl groups in CTA. Peaks at 1.8–2.2 ppm correlate to the methyl protons of CTA acetyl groups (El Nemr et al. 2015). Peaks at higher ppm, around 3.4–5.2 ppm, were peaks of seven anhydroglucose unit protons (Nemr et al. 2017). A proton signal paired to the C5 atom was detected at 3.55 ppm, 3.7 ppm for C4, 4.07 ppm for C6, 4.4 ppm for C1 and C6', 4.79 ppm for C2 and 5.07 ppm for C3. The peaks were similar to CTA produced from microfibrillated date seeds, date palm trunk mesh, bleached eucalyptus pulp and bleached *Pinus* pulp (Malucelli et al. 2020; Nabili et al. 2017; Shaikh et al. 2022). No peaks presented at 5.5–6.5 ppm, showing that the DS of CTA was theoretically ≥ 3 since no resonance of α,β-anomeric protons of reducing end residues that would normally appear in that area (Nabili et al. 2017). A peak from the deuterated chloroform, as the solvent, was observed at around 7.2 ppm. The DS of CTA based on $^{1}$H-NMR was 2.99 confirming the CTA produced. This means all the hydroxyl groups in C2, C3 and C6 were acetylated. The DS value was also in agreement with the DS value obtained by titration.

Furthermore, $^{13}$C-NMR spectra are shown in Fig. 6b and 6c. A singlet carbon ring of CTA showed that the CTA produced was CTA-I, which are allomorphs of cellulose and CTA (Nabili et al. 2017). Carbon atoms in carbonyl groups (-C = O) are indicated between 169 and 171 ppm. The first carbon atom is located at around 100–101 ppm where C2-C5 are distributed between 71 and 76 ppm. C6, on the other hand, was located at 62 ppm. Carbon atoms in -$COOCH_3$ were located at 20–21 ppm.

# Morphology visualization

Field emission scanning electron microscopy (FESEM) was used to visualize the raw kapok fibre, delignified kapok fibre and CTA. As shown in Fig. 7, raw kapok fibre exhibited a non-porous and smooth surface whilst delignified kapok fibre exhibited a rougher surface with pores. At this stage, raw kapok fibres were still covered with a waxy layer. The smooth silky surface was similar to that reported by Fauziah Syed Draman et al. (2014). Pores were formed after delignification where lignin and hemicellulose, which are the building materials that provide rigidity and strength, were broken down and dissolved, leaving behind a more open and porous structure. The delignified fibres became flat in shape but remained unbroken. On the other hand, CTA appeared as a fine, white powder, and was typically very small and irregular in shape. Spheres, interconnected fibres, and some irregular shapes were scattered around the CTA and exhibited roughness and textured properties. Visually, the porosity of CTA is much higher than that of the delignified kapok fibre, with visible micropores, thus making it suitable as an additive to improve porosity of a membrane.

# Porosity

In crude oil absorption, membranes must possess particular characteristics including good permeability and high surface area. Membrane permeability is heavily dependent on porosity and pore size (Ali et al. 2018; Kasemset et al. 2017; Rekik et al. 2017). Moderate porosity is desired as high porosity decreases the pore size, and vice versa, which may hinder the absorption of crude oil. At the same time, porosity, pore size and pore size distribution are related to the surface area of the membrane which determines the absorption capacity. Surface roughness also influences membrane permeability and surface area (AlMarzooqi et al. 2016; Gao et al. 2019).

Porosity refers to the volume of pores to the total volume of the membrane (Saini et al. 2019). In this study, the porosity was measured using the gravimetric method. Figure 8 revealed that the highest porosity was from membrane PC2 with 85.75% porosity. PC2 showed no significant differences to PC1, PC3, PC4 and PC5 whose porosity ranged from 84.57%-85.75%. The lowest porosity was PC0.01 and PC0.05 with values of 65.66% and 66.96%, respectively. The neat PVDF membrane (PC0) had a porosity of 68.82% which was higher than those reported in previous studies. Pure PVDF membrane has been reported to vary in porosity. Water-induced phase inversion PVDF membrane showed 75% porosity while another one reported 55.6% porosity (Hai et al. 2019; Zhu et al. 2015). PVDF with high molecular weight would produce membranes with higher porosity (Chen et al. 2015). However, this was in contradiction with the typical results which showed that high molecular weight polymer will result in porous membrane with low porosity.

# Crude oil absorption

Ten mL of crude oil was used to ensure full immersion of the membrane. The crude oil absorption capacity can be seen in Fig. 9. PC0.01 was chosen since the porosity was significantly higher than PC0, while PC0.5 and PC3 were significantly higher. However, in terms of absorption capacity, PC0.01 and PC0.5 were not significant different to PC0, whereas PC3 absorbed significantly higher. PC0, PC0.01 and PC0.5 could absorb around 169%, 181% and 178% of its dry weight, respectively. Moreover, PC3 could

absorb up to 265% of its dry weight. High porosity usually allows more absorption or permeation of substances with its many open pores. Other than porosity, pore size, material composition and surface chemistry influence the selectivity of which substances can be absorbed (Padaki et al. 2015).

As most membranes were used to either filter or separate the crude oil emulsion from contaminated seawater, there is not much information on the membrane solely being used to only absorb crude oil. Polyvinylidene fluoride/SiO2@graphene oxide (PVDF/SiO2@GO) aerogels showed an excellent crude oil absorption capacity of 129–264 g/g (Wang et al. 2022). Research used cross-linked chitosan aerogel as a crude oil absorbent with 41.07 g/g maximum capacity (Li et al. 2016). An absorbent made of nano porous graphene polyurethane had a crude oil absorption capacity of 70 g/g (Rahmani et al. 2017). This showed that the produced PVDF/CTA membrane had a very low crude oil absorption capacity in comparison with the established absorbent.

# Conclusion

In this study, kapok fibre was used to produce CTA since it is cheaper, easier to make and has fewer environmental impacts (such as deforestation) compared to CTA produced from woods. Raw kapok fibre was delignified and bleached prior to acetylation. Based on the characterizations, the produced CTA was confirmed to have a DS of 2.9 which is in the range of DS for cellulose triacetate that is also soluble in chloroform. FTIR detected the disappearance of hydroxyl groups and the appearance of acetyl groups in the CTA product. The thermal properties of CTA were characterized by TGA and DSC, where crystallinity was determined by XRD. Both $^{1}$H-NMR and $^{13}$C-NMR were done to confirm the CTA produced by looking at the molecular conformation. Under FeSEM, the smooth appearance of raw kapok fibre was converted into slightly porous delignified kapok fibre until it reached the stage of porous CTA. The porous CTA significantly increased the porosity of PVDF/CTA membrane as the concentration of CTA went up thus improve its absorption capacity towards crude oil. Studies are currently underway to try immobilizing oil-degrading bacteria to achieve concurrent absorption and degradation of crude oil spills.

# Declarations

Author Contributions

L.A wrote the main manuscript text and carried out the experimentation. E.C.W.C. provided guidance on experimentation and co-supervised L.A. J.J. provided co-supervision to L.A., funded part of the experimentation and reviewed the manuscript. J.B. reviewed the manuscript critically and provided suggestions for improvements. M.S.O.Y. supervised L.A research, provided the main funding for the experimentation (recipient of the FRGS grant) and reviewed the manuscript.

Funding

This research was supported by funding from Fundamental Research Grant Scheme (FRGS) by the Ministry of Higher Education (FRGS/1/2019/STG05/UCSI/03/1), an internal university grant (PSIF grant

No. PROJ-2019-In-FAS-063) of UCSI University KL and Geran Induk Higher Education Center of Excellence (HICoE) Advanced Membrane Technology Research Centre (AMTEC) (A.J091400.6800.07092).

Data Availability

All relevant data is within the manuscript.

Ethical Approval

No ethical approval was needed for this study.

Competing Interests

The authors have no relevant financial or non-financial competing interests to disclose.

# References

1. Ali I, Bamaga OA, Gzara L, et al (2018) Assessment of Blend PVDF Membranes, and the Effect of Polymer Concentration and Blend Composition. Membranes 2018, Vol 8, Page 13 8:13. https://doi.org/10.3390/MEMBRANES8010013
2. AlMarzooqi FA, Bilad MR, Mansoor B, Arafat HA (2016) A comparative study of image analysis and porometry techniques for characterization of porous membranes. J Mater Sci 51:2017–2032. https://doi.org/10.1007/S10853-015-9512-0/FIGURES/9
3. Battisti R, Hafemann E, Antonio R, et al (2018) Synthesis and characterization of cellulose acetate from royal palm tree agroindustrial waste. Polym Eng Sci 59:891–898. https://doi.org/10.1002/pen.25034
4. Boukir A, Mehyaoui I, Fellak S, et al (2019) The effect of the natural degradation process on the cellulose structure of Moroccan hardwood fiber: a survey on spectroscopy and structural properties. Mediterranean Journal of Chemistry 8:179–190. https://doi.org/10.13171/MJC8319050801AB
5. Bouramdane Y, Fellak S, El Mansouri F, Boukir A (2022) Impact of Natural Degradation on the Aged Lignocellulose Fibers of Moroccan Cedar Softwood: Structural Elucidation by Infrared Spectroscopy (ATR-FTIR) and X-ray Diffraction (XRD). Fermentation 2022, Vol 8, Page 698 8:698. https://doi.org/10.3390/FERMENTATION8120698
6. Chan EWC, Yeong SW, Wong CW, et al (2022) Ceiba pentandra (L.) Gaertn.: An overview of its botany, uses, reproductive biology, pharmacological properties, and industrial potentials. https://doi.org/10.7324/JABB.2023.110101

7. Chen Z, Rana D, Matsuura T, et al (2015) Study on structure and vacuum membrane distillation performance of PVDF membranes: II. Influence of molecular weight. Chemical Engineering Journal 276:174–184. https://doi.org/10.1016/J.CEJ.2015.04.030
8. Cobo FN, Faria-Tisher PCS, Duarte JL, Carvalho GM (2017) Preparation and characterization of microporous cellulose acetate films using breath figure method by spin coating technique. Cellulose 24:4981–4995. https://doi.org/10.1007/S10570-017-1459-7
9. Danial Jamat M, Asik J (2019) PERFORMANCE OF KAPOK FIBER REINFORCED POLYVINYL ALCOHOL BICOMPOSITE BY ALKALI TREATED. BORNEO SCIENCE 40:38–50
10. de Freitas RRM, Senna AM, Botaro VR (2017) Influence of degree of substitution on thermal dynamic mechanical and physicochemical properties of cellulose acetate. Ind Crops Prod 109:452–458. https://doi.org/10.1016/J.INDCROP.2017.08.062
11. de Melo Brites M, Cerón AA, Costa SM, et al (2020) Bromelain immobilization in cellulose triacetate nanofiber membranes from sugarcane bagasse by electrospinning technique. Enzyme Microb Technol 132:109384. https://doi.org/10.1016/J.ENZMICTEC.2019.109384
12. Dong F, Yan M, Jin C, Li S (2017) Characterization of Type-II Acetylated Cellulose Nanocrystals with Various Degree of Substitution and Its Compatibility in PLA Films. Polymers 2017, Vol 9, Page 346 9:346. https://doi.org/10.3390/POLYM9080346
13. El Nemr A, Ragab S, El Sikaily A, Khaled A (2015) Synthesis of cellulose triacetate from cotton cellulose by using NIS as a catalyst under mild reaction conditions. Carbohydr Polym 130:41–48. https://doi.org/10.1016/J.CARBPOL.2015.04.065
14. Estefania A, Loor V (2022) Novel use of hydrogen peroxide to convert bleached kraft pulp into dissolving pulp and microfibrillated cellulose.
15. Fauziah Syed Draman S, Daik R, Abdul Latif F, et al (2014) Characterization and Thermal Decomposition Kinetics of Kapok (Ceiba pentandra L.)-Based Cellulose. Bioresources 9:8–23
16. Fei P, Liao L, Cheng B, Song J (2017) Quantitative analysis of cellulose acetate with a high degree of substitution by FTIR and its application. Analytical Methods 9:6194–6201. https://doi.org/10.1039/C7AY02165H
17. Gao F, Wang J, Zhang H, et al (2019) Aged PVDF and PSF ultrafiltration membranes restored by functional polydopamine for adjustable pore sizes and fouling control. J Memb Sci 570–571:156–167. https://doi.org/10.1016/J.MEMSCI.2018.10.037
18. Gomide RAC, de Oliveira ACS, Rodrigues DAC, et al (2020) Development and Characterization of Lignin Microparticles for Physical and Antioxidant Enhancement of Biodegradable Polymers. J Polym Environ 28:1326–1334. https://doi.org/10.1007/S10924-020-01685-Z
19. Guo F, Wu F, Mu Y, et al (2016) Characterization of organic matter of plants from lakes by thermal analysis in a N2 atmosphere. Scientific Reports 2016 6:1 6:1–7. https://doi.org/10.1038/srep22877
20. Hai A, Durrani AA, Selvaraj M, et al (2019) Oil-water emulsion separation using intrinsically superoleophilic and superhydrophobic PVDF membrane. Sep Purif Technol 212:388–395. https://doi.org/10.1016/J.SEPPUR.2018.10.001

21. Hindi SSZ, Abohassan RA (2015) Cellulose Triacetate Synthesis from Cellulosic Wastes by Heterogeneous Reactions. Bioresources 10:5030–5048
22. Jia X, Guo D, Yan Q, et al (2022) Synthesis and Characterization of Corn Stover-Based Cellulose Triacetate Catalyzed by Ionic Liquid Phosphotungstate. International Journal of Molecular Sciences 2022, Vol 23, Page 6783 23:6783. https://doi.org/10.3390/IJMS23126783
23. Jogunola O, Eta V, Hedenström M, et al (2016) Ionic liquid mediated technology for synthesis of cellulose acetates using different co-solvents. Carbohydr Polym 135:341–348. https://doi.org/10.1016/j.carbpol.2015.08.092
24. Joshi P, Roy R, Rahman S, et al (2022) Recent Advances in Lignin Depolymerization Techniques: A Comparative Overview of Traditional and Greener Approaches. Biomass 2022, Vol 2, Pages 130-154 2:130–154. https://doi.org/10.3390/BIOMASS2030009
25. Jun Poon J, Ching Tan M, Loo Kiew P (2020) ULTRASOUND-ASSISTED EXTRACTION IN DELIGNIFICATION PROCESS TO OBTAIN HIGH PURITY CELLULOSE. CELLULOSE CHEMISTRY AND TECHNOLOGY Cellulose Chem Technol 54:725–734
26. Kang ZY, Zachariah JA, Chan EWC, Soo MOY (2022) Modification of kapok cotton fibres into porous cellulose triacetate beads for oil spill remediation. https://doi.org/101680/jgrma2100064. https://doi.org/10.1680/JGRMA.21.00064
27. Kasemset S, Wang L, He Z, et al (2017) Influence of polydopamine deposition conditions on hydraulic permeability, sieving coefficients, pore size and pore size distribution for a polysulfone ultrafiltration membrane. J Memb Sci 522:100–115. https://doi.org/10.1016/J.MEMSCI.2016.07.016
28. Kumar A, Jyske T, Petrič M (2021) Delignified Wood from Understanding the Hierarchically Aligned Cellulosic Structures to Creating Novel Functional Materials: A Review. Adv Sustain Syst 5:2000251. https://doi.org/10.1002/ADSU.202000251
29. Kumar R, Sharma RK, Singh AP (2017) Cellulose based grafted biosorbents - Journey from lignocellulose biomass to toxic metal ions sorption applications - A review. J Mol Liq 232:62–93. https://doi.org/10.1016/J.MOLLIQ.2017.02.050
30. Li A, Lin R, Lin C, et al (2016) An environment-friendly and multi-functional absorbent from chitosan for organic pollutants and heavy metal ion. Carbohydr Polym 148:272–280. https://doi.org/10.1016/J.CARBPOL.2016.04.070
31. Malucelli LC, Lomonaco D, Filho MASC, Magalhães WLE (2020) Cellulose triacetate from different sources: Modification assessment through thermal and chemical characterization. Holzforschung 74:505–512. https://doi.org/10.1515/HF-2019-0035/MACHINEREADABLECITATION/RIS
32. Mittal A, Katahira R, Himmel ME, Johnson DK (2011) Effects of alkaline or liquid-ammonia treatment on crystalline cellulose: Changes in crystalline structure and effects on enzymatic digestibility. Biotechnol Biofuels 4:1–16. https://doi.org/10.1186/1754-6834-4-41/FIGURES/9
33. Mohamed MA, Salleh WNW, Jaafar J, et al (2017) Physicochemical characterization of cellulose nanocrystal and nanoporous self-assembled CNC membrane derived from Ceiba pentandra.

Carbohydr Polym 157:1892–1902. https://doi.org/10.1016/J.CARBPOL.2016.11.078

34. Nabili A, Fattoum A, Brochier-Salon MC, et al (2017) Synthesis of cellulose triacetate-I from microfibrillated date seeds cellulose (Phoenix dactylifera L.). Iranian Polymer Journal (English Edition) 26:137–147. https://doi.org/10.1007/S13726-017-0505-5/METRICS
35. Nemr A El, Ragab S, Sikaily A El (2017) Rapid synthesis of cellulose triacetate from cotton cellulose and its effect on specific surface area and particle size distribution. Iranian Polymer Journal (English Edition) 26:261–272. https://doi.org/10.1007/S13726-017-0516-2/FIGURES/8
36. Nindiyasari F, Griesshaber E, Zimmermann T, et al (2016) Characterization and mechanical properties investigation of the cellulose/gypsum composite. J Compos Mater 50:657–672. https://doi.org/10.1177/0021998315580826
37. Nordahlia AS, Noraini T, Chung RCK, et al (2016) Comparative wood anatomy of three Bombax species and Ceiba pentandra (Malvaceae: Bombacoideae) in Malaysia. Malayan Nature Journal 1784:. https://doi.org/10.1063/1.4966868
38. Nu DTT, Hung NP, Van Hoang C, Van der Bruggen B (2019) Preparation of an asymmetric membrane from sugarcane bagasse using DMSO as green solvent. Applied Sciences (Switzerland) 9:. https://doi.org/10.3390/APP9163347
39. Padaki M, Surya Murali R, Abdullah MS, et al (2015) Membrane technology enhancement in oil–water separation. A review. Desalination 357:197–207. https://doi.org/10.1016/J.DESAL.2014.11.023
40. Purnawati R, Febrianto F, Wistara INJ, et al (2018) Physical and Chemical Properties of Kapok (Ceiba pentandra) and Balsa (Ochroma pyramidale) Fibers. Journal of the Korean Wood Science and Technology 46:393–401. https://doi.org/10.5658/WOOD.2018.46.4.393
41. Rahim A, Kadir S, Jusman (2017) The influence degree of substitution on the physicochemical properties of acetylated arenga starches. Int Food Res J 24:102–107
42. Rahmah AU, Abdullah MA (2011) Evaluation of Malaysian Ceiba pentandra (L.) Gaertn. for oily water filtration using factorial design. Desalination 266:51–55. https://doi.org/10.1016/J.DESAL.2010.08.001
43. Rahmani Z, Samadi MT, Kazemi A, et al (2017) Nanoporous graphene and graphene oxide-coated polyurethane sponge as a highly efficient, superhydrophobic, and reusable oil spill absorbent. J Environ Chem Eng 5:5025–5032. https://doi.org/10.1016/J.JECE.2017.09.028
44. Rekik SB, Gassara S, Bouaziz J, et al (2017) Development and characterization of porous membranes based on kaolin/chitosan composite. Appl Clay Sci 143:1–9. https://doi.org/10.1016/J.CLAY.2017.03.008
45. Saini B, Sinha MK, Dash SK (2019) Mitigation of HA, BSA and oil/water emulsion fouling of PVDF Ultrafiltration Membranes by SiO2-g-PEGMA nanoparticles. Journal of Water Process Engineering 30:100603. https://doi.org/10.1016/J.JWPE.2018.03.018
46. Sartika D, Syamsu K, Warsiki E, Fahma F (2020) Isolation of microfiber cellulose from kapok fiber (Ceiba pentandra) by using chemical-hydrothermal treatment. Ecology, Environment and

Conservation 26:654–662

47. Shaikh HM, Anis A, Poulose AM, et al (2022) Synthesis and Characterization of Cellulose Triacetate Obtained from Date Palm (Phoenix dactylifera L.) Trunk Mesh-Derived Cellulose. Molecules 2022, Vol 27, Page 1434 27:1434. https://doi.org/10.3390/MOLECULES27041434
48. Susi S, Ainuri M, Wagiman W, et al (2023a) Depolymerization of Cellulose Components from Oil Palm Empty Fruit Bunches in Bleaching and Delignification Process. Engineering Chemistry 4:41–49. https://doi.org/10.4028/P-UGJQS1
49. Susi S, Ainuri M, Wagiman W, Falah MAF (2023b) High-Yield Alpha-Cellulose from Oil Palm Empty Fruit Bunches by Optimizing Thermochemical Delignification Processes for Use as Microcrystalline Cellulose. Int J Biomater 2023:. https://doi.org/10.1155/2023/9169431
50. Suzuki S, Shibata Y, Hirose D, et al (2018) Cellulose triacetate synthesis via one-pot organocatalytic transesterification and delignification of pretreated bagasse. RSC Adv 8:21768–21776. https://doi.org/10.1039/C8RA03859G
51. Tristantini D, Sandra C (2018) Synthesis of cellulose acetate from palm oil bunches and dried jackfruit leaves. E3S Web of Conferences 67:04035. https://doi.org/10.1051/E3SCONF/20186704035
52. Velu S, Muruganandam L, Arthanareeswaran G (2015) PREPARATION AND PERFORMANCE STUDIES ON POLYETHERSULFONE ULTRAFILTRATION MEMBRANES MODIFIED WITH GELATIN FOR TREATMENT OF TANNERY AND DISTILLERY WASTEWATER. Brazilian Journal of Chemical Engineering 32:179–189. https://doi.org/10.1590/0104-6632.20150321S00002965
53. Wang X, Liu Z, Liu X, et al (2022) Ultralight and multifunctional PVDF/SiO2@GO nanofibrous aerogel for efficient harsh environmental oil-water separation and crude oil absorption. Carbon N Y 193:77–87. https://doi.org/10.1016/J.CARBON.2022.03.028
54. Wolfs J, Meier MAR (2021) A more sustainable synthesis approach for cellulose acetate using the DBU/CO 2 switchable solvent system. Green Chemistry 23:4410–4420. https://doi.org/10.1039/D1GC01508G
55. Wsoo MA, Shahir S, Mohd Bohari SP, et al (2020) A review on the properties of electrospun cellulose acetate and its application in drug delivery systems: A new perspective. Carbohydr Res 491:107978. https://doi.org/10.1016/J.CARRES.2020.107978
56. Xiang HF, Wang D, Liua HC, et al (2013) Investigation on sound absorption properties of kapok fibers. Chinese Journal of Polymer Science (English Edition) 31:521–529. https://doi.org/10.1007/S10118-013-1241-8/METRICS
57. Yang WD, Li Y (2012) Sound absorption performance of natural fibers and their composites. Sci China Technol Sci 55:2278–2283. https://doi.org/10.1007/S11431-012-4943-1/METRICS
58. Yang Z, Yan J, Wang F (2018) Pore structure of kapok fiber. Cellulose 25:3219–3227. https://doi.org/10.1007/S10570-018-1767-6/FIGURES/11
59. Yuan X, Cheng G (2015) From cellulose fibrils to single chains: understanding cellulose dissolution in ionic liquids. Physical Chemistry Chemical Physics 17:31592–31607.

https://doi.org/10.1039/C5CP05744B

60. Yuan Y, Jiang B, Chen H, et al (2021) Recent advances in understanding the effects of lignin structural characteristics on enzymatic hydrolysis. Biotechnology for Biofuels 2021 14:1 14:1–20. https://doi.org/10.1186/S13068-021-02054-1
61. Yunita RF, Nasution DY, Marpongahtun (2018) Manufacturing & Characterization of Cellulose Acetate Film from Oil Palm Logs (Elaeis Guinensis Jack) with Chloroform as Solvent & Triacetin as Plasticizer. IJSTE-International Journal of Science Technology & Engineering | 4:
62. Zhang S, Yang Z, Huang X, et al (2022) Hydrophobic Cellulose Acetate Aerogels for Thermal Insulation. Gels 2022, Vol 8, Page 671 8:671. https://doi.org/10.3390/GELS8100671
63. Zhang X, Zhang F, Li P, Tong G (2023) Synthesis of cellulose triacetate from softwood dissolving pulp using p-toluenesulfonic acid and its properties. Cellulose 30:6787–6797. https://doi.org/10.1007/S10570-023-05294-6/FIGURES/6
64. Zheng Y, Wang J, Zhu Y, Wang A (2015) Research and application of kapok fiber as an absorbing material: A mini review. Journal of Environmental Sciences 27:21–32. https://doi.org/10.1016/J.JES.2014.09.026
65. Zhou H, Tong H, Lu J, et al (2021) Preparation of bio-based cellulose acetate/chitosan composite film with oxygen and water resistant properties. Carbohydr Polym 270:118381. https://doi.org/10.1016/J.CARBPOL.2021.118381
66. Zhou X, Lin X, White KL, et al (2016) Effect of the degree of substitution on the hydrophobicity of acetylated cellulose for production of liquid marbles. Cellulose 23:811–821. https://doi.org/10.1007/S10570-015-0856-Z/FIGURES/7
67. Zhu Y, Xie W, Li J, et al (2015) pH-Induced non-fouling membrane for effective separation of oil-in-water emulsion. J Memb Sci 477:131–138. https://doi.org/10.1016/J.MEMSCI.2014.12.026

## Table

Table 3 is available in the Supplementary Files section.

## Figures

a

b

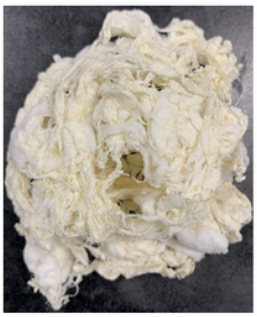

c

d

## Figure 1

picture of: a) raw kapok fibre; b) delignified kapok fibre (before bleaching); c) delignified kapok fibre (after bleaching); d) cellulose triacetate

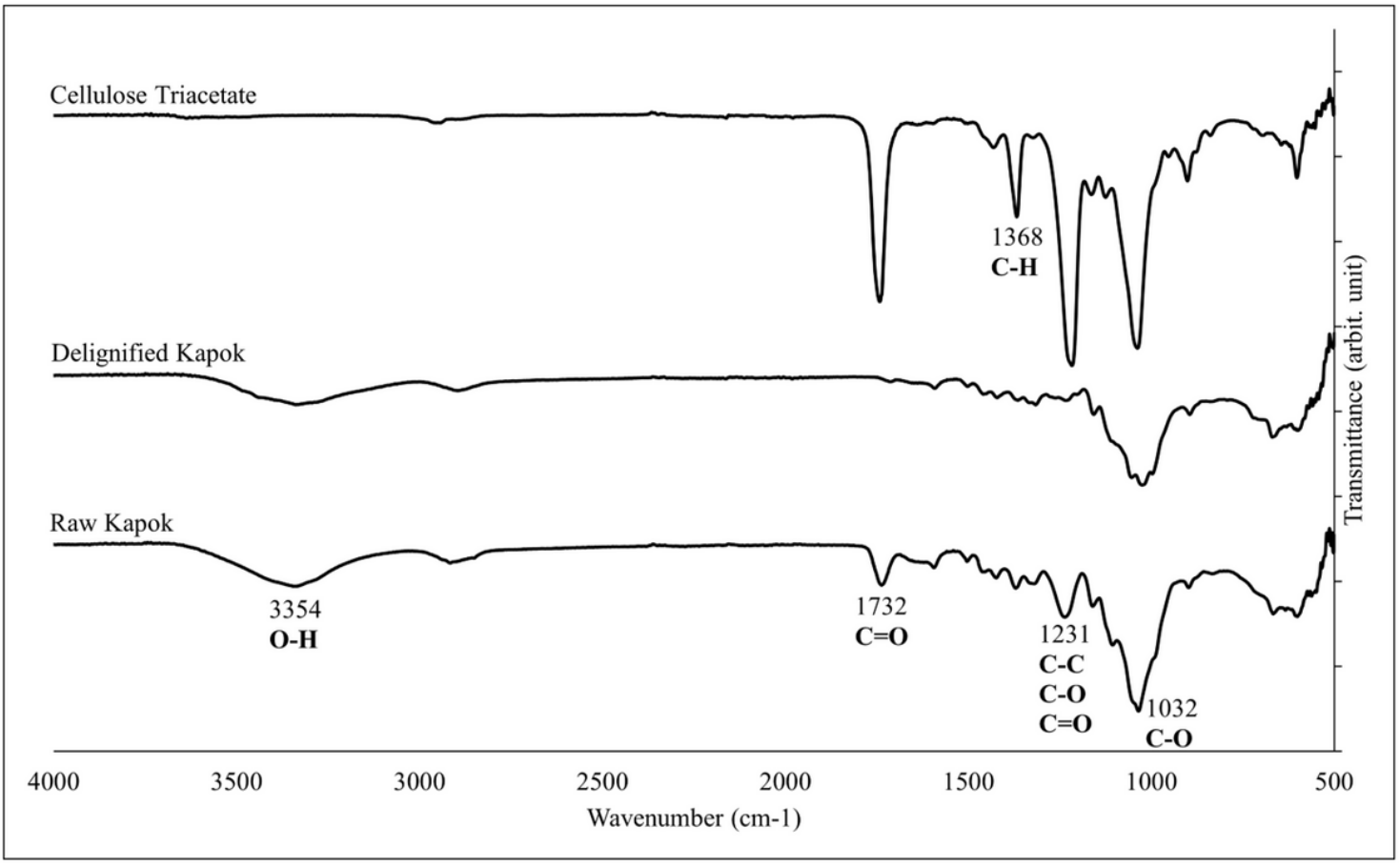


## Figure 2

FTIR spectrum of raw kapok fibres, delignified kapok fibres and CTA.

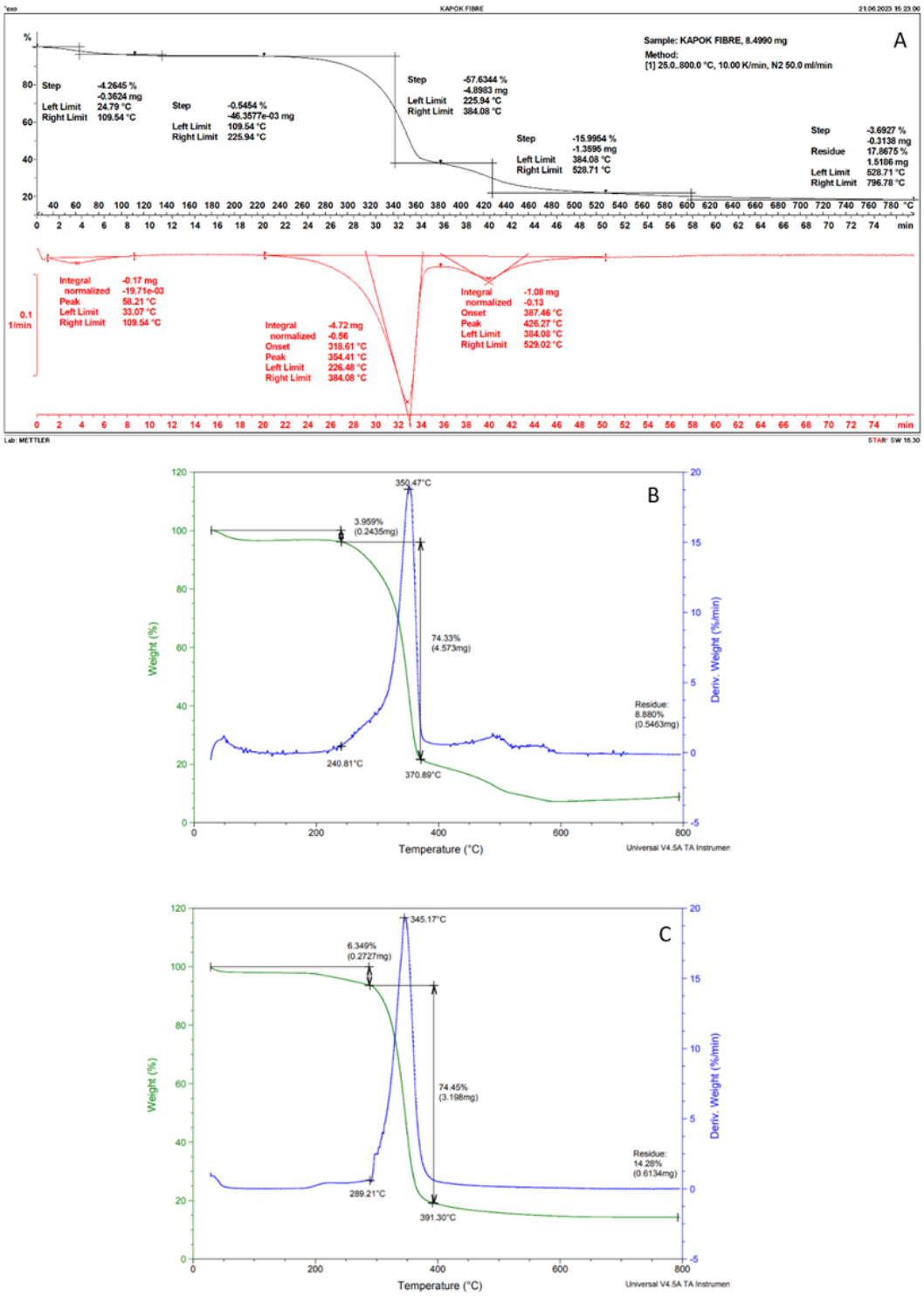


## Figure 3

Thermogravimetric analysis and differential thermogravimetric curves of: a) raw kapok fibres; b) delignified kapok fibres; c) CTA. Note that Figure 3a was obtained from a different instrument that has a different way of presenting the results.

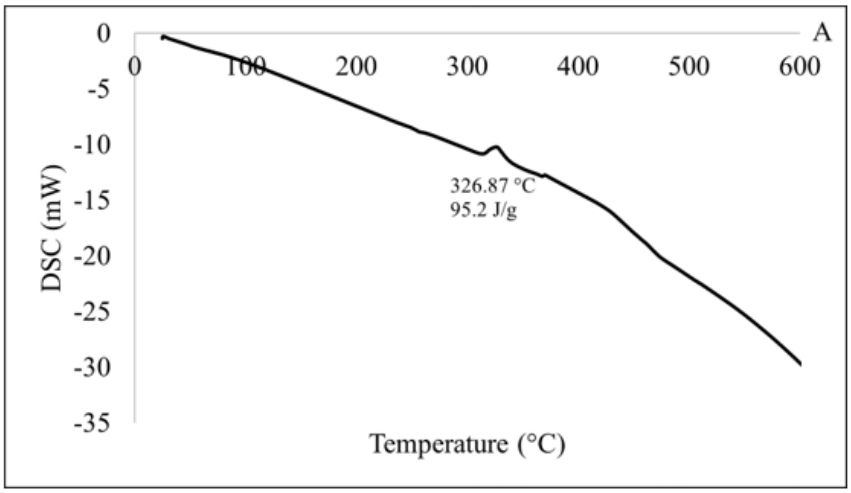


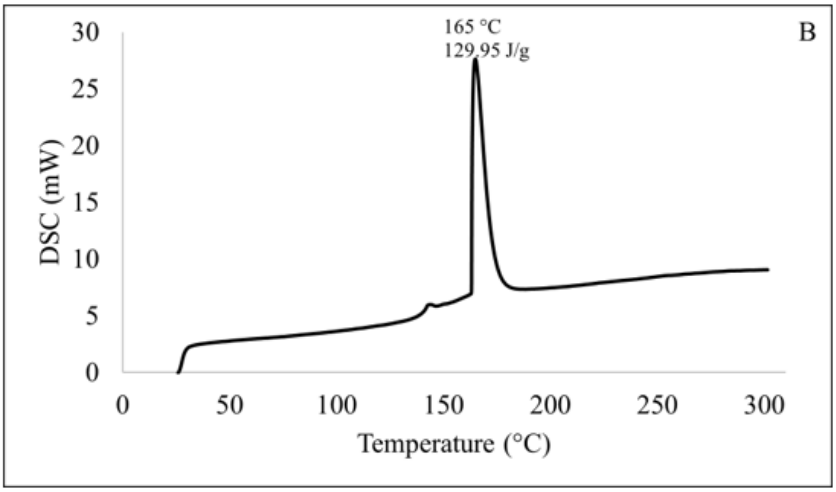


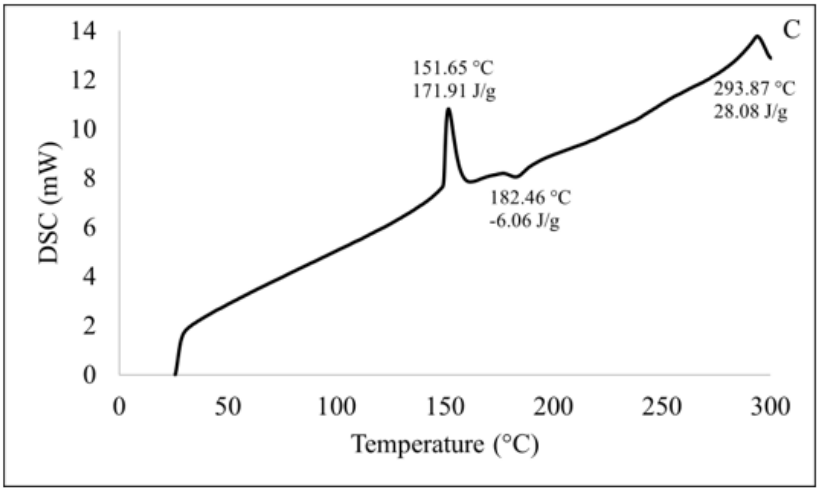


## Figure 4

Differential scanning calorimetry (DSC) results of: a) raw kapok fibres; b) delignified kapok fibres; c) CTA. It should be noted that Figure 4a was obtained from a different instrument where the sample was heated up to 800 °C whereas the other samples were heated up to 300 °C.

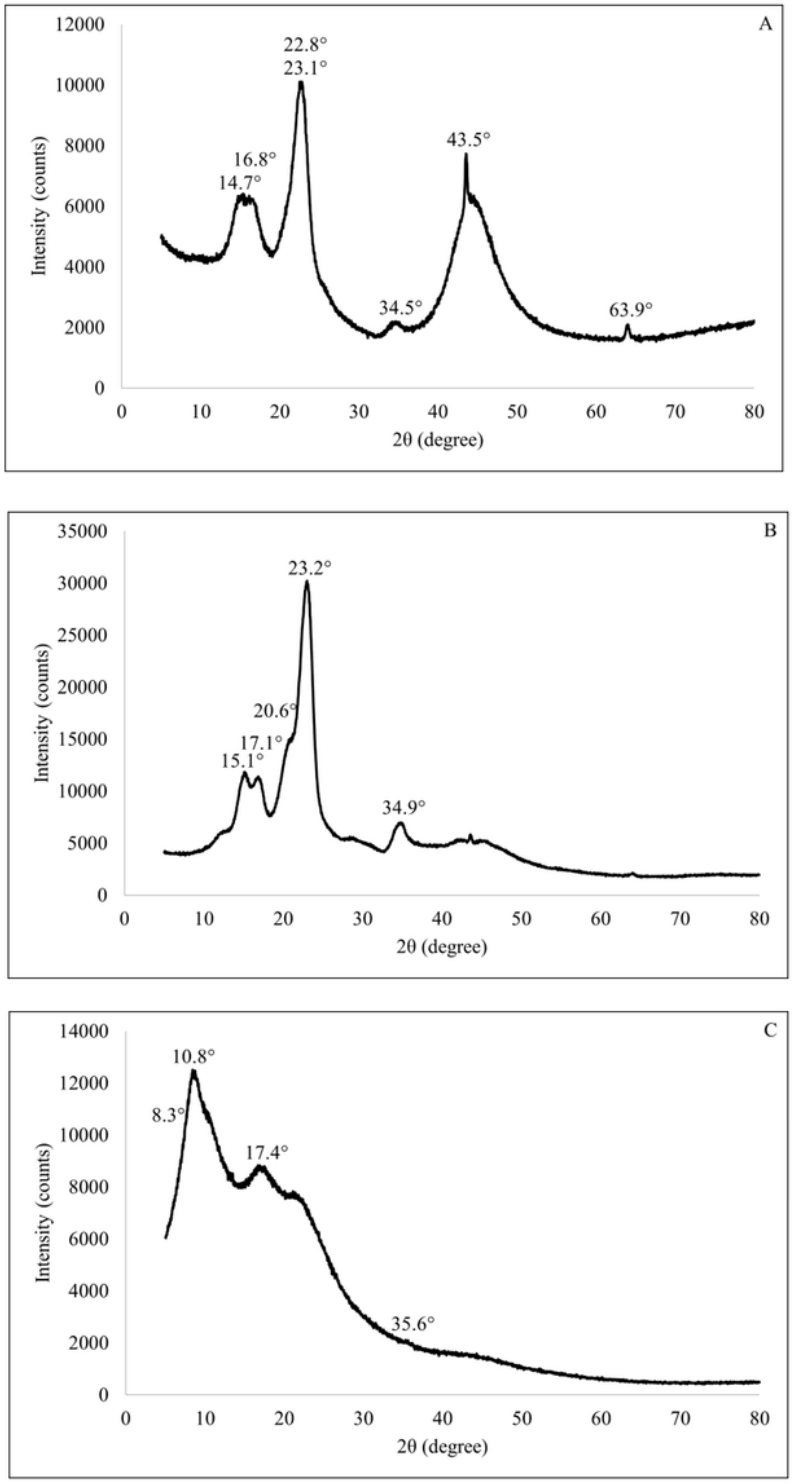


## Figure 5

X-ray diffraction pattern of: a) raw kapok fibres; b) delignified kapok fibres; c) CTA

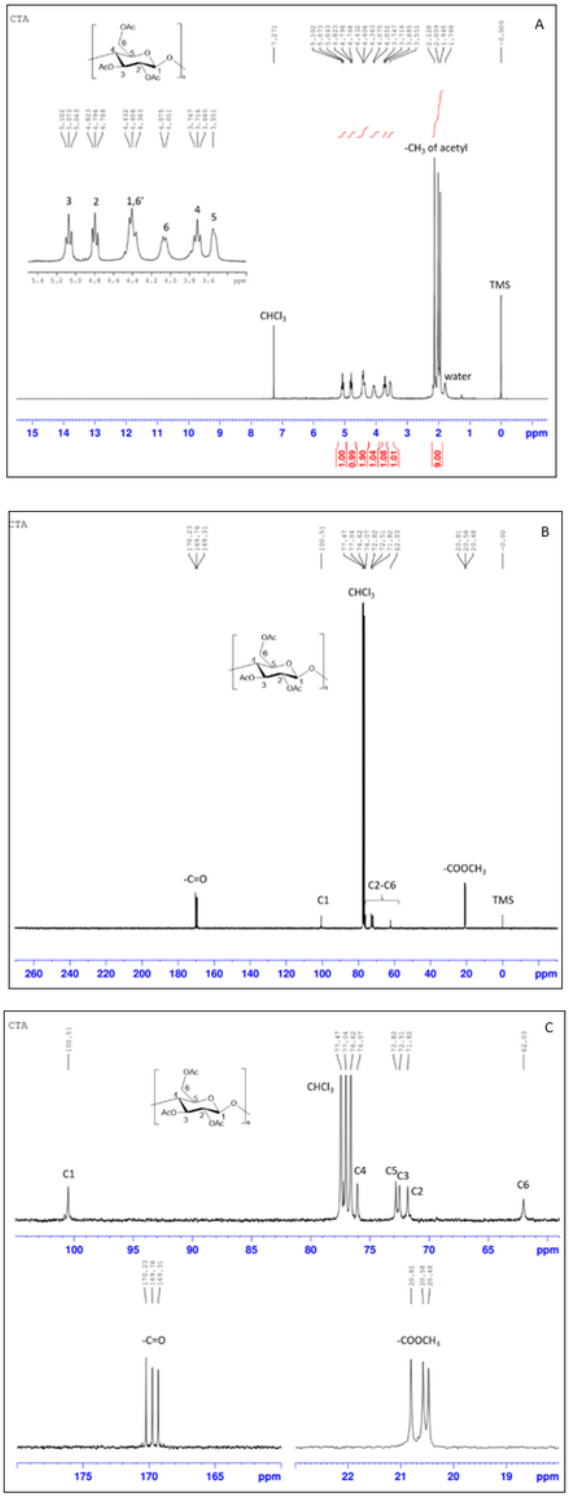


## Figure 6

NMR spectra of cellulose triacetate: a) H-NMR; b) C-NMR; c) C-NMR (zoomed in)

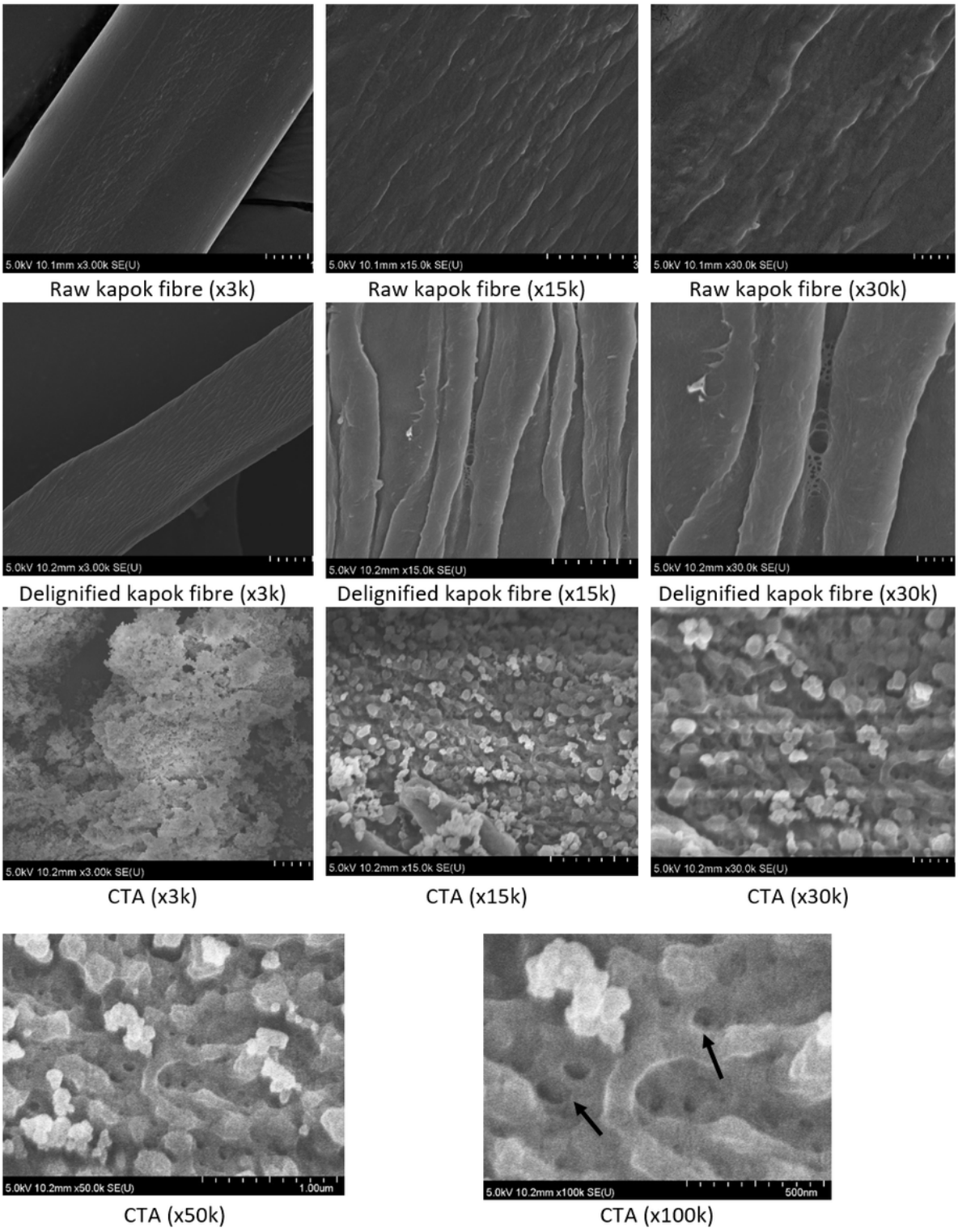


## Figure 7

Field emission scanning electron microscopy characterization of raw kapok fibres, delignified kapok fibres and cellulose triacetate.

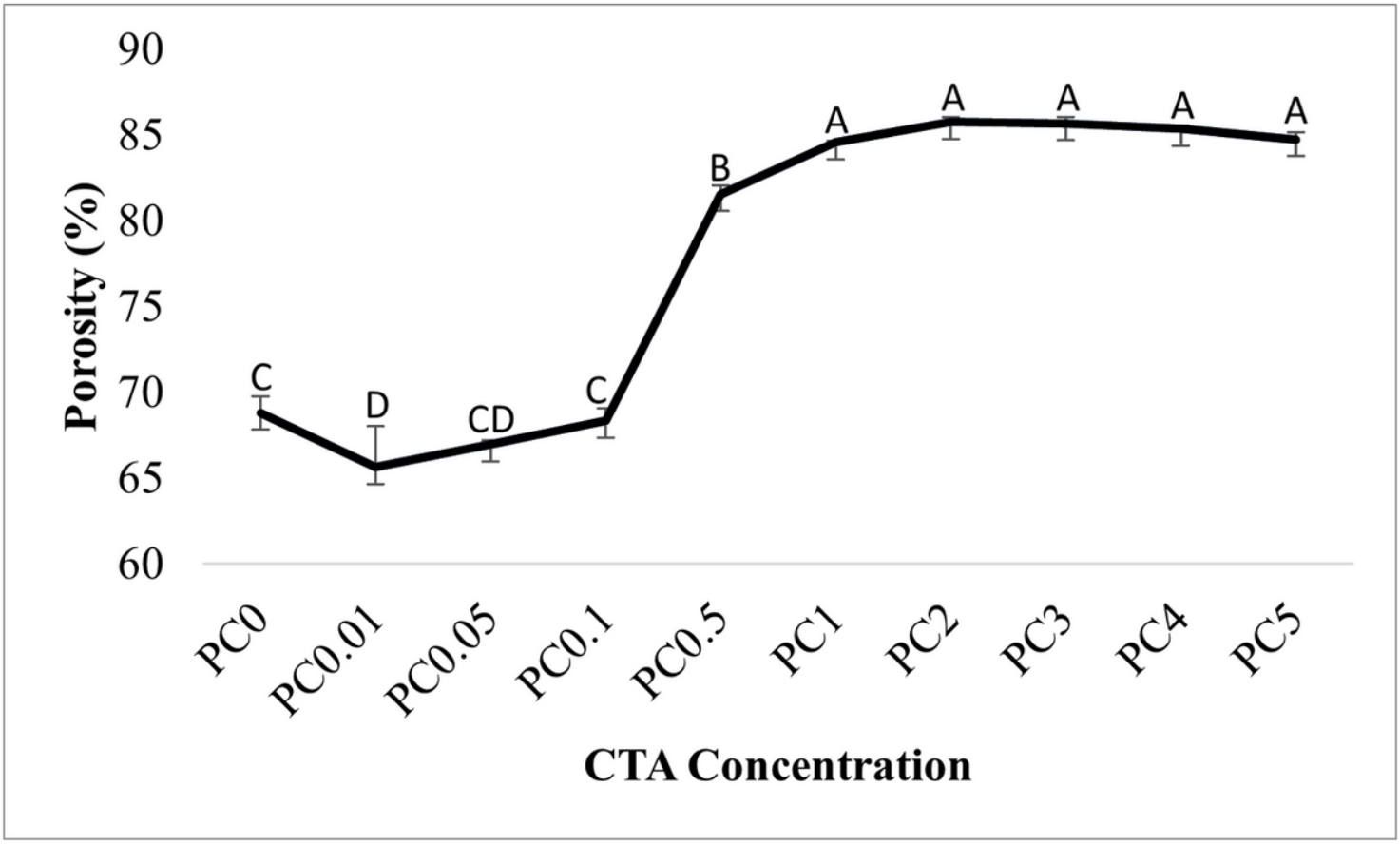


## Figure 8

The porosity of PVDF membrane combined with different concentrations of CTA. Mean values that do not share the letters (A-D) are significantly different.

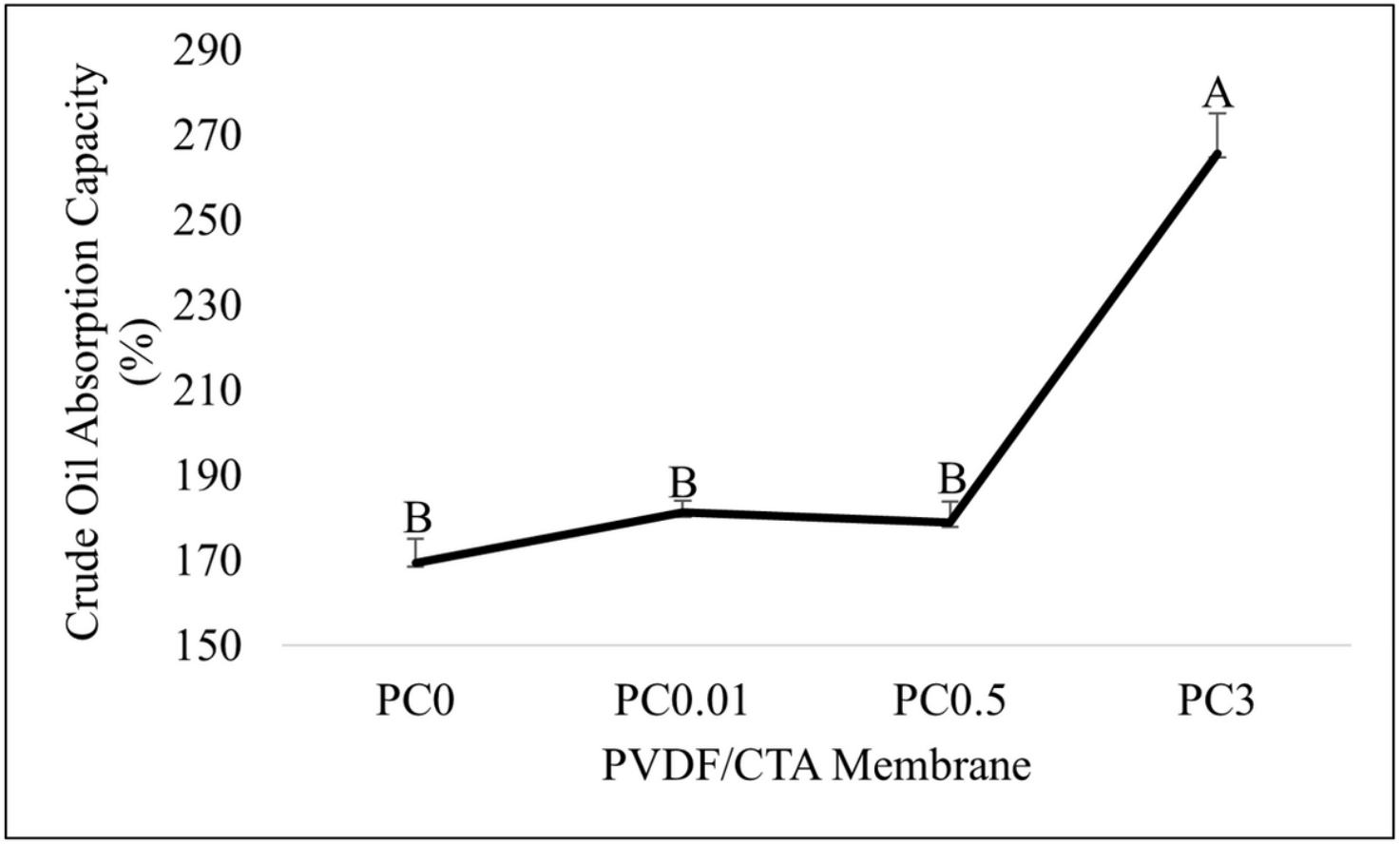


**Figure 9**

Crude oil absorption capacity of PVDF/CTA membrane. Mean values that do not share the same letters (A-B) are significantly different.

## Supplementary Files

This is a list of supplementary files associated with this preprint. Click to download.

- Table3.docx